

Hyperspectral Image Classification Using Orthogonal Subspace Projections: Image Simulation and Noise Analysis

Emmett Ientilucci, Center for Imaging Science

April 23, 2001

Contents

| | | |
|----------|---|-----------|
| 1 | Introduction | 4 |
| 2 | Background | 4 |
| 2.1 | Remote Sensing: An Overview | 4 |
| 2.2 | Sensors and Imaging Spectrometers | 5 |
| 2.3 | Classification Techniques and Transforms | 6 |
| 3 | Orthogonal Subspace Projection Classification | 7 |
| 3.1 | Problem Formation | 7 |
| 3.2 | Hyperspectral Pixel Classification | 8 |
| 3.2.1 | Interference Rejection by Orthogonal Subspace Pro- jection | 8 |
| 3.2.2 | Signal-to-Noise Ratio (SNR) Maximization | 9 |
| 4 | 100 Pixel Simulated Scene | 10 |
| 4.1 | Scene Overview | 10 |
| 4.2 | OSP Formulation and Results for One Pixel w/o Noise | 12 |
| 4.3 | OSP Results for Test Image with out Noise | 15 |
| 4.4 | OSP Results for Test Image with Noise | 16 |
| 4.4.1 | 1% Gaussian Noise | 16 |
| 4.4.2 | 5% Gaussian Noise | 17 |
| 4.5 | Classified Concrete Image: A Closer Look at Noise | 19 |
| 4.5.1 | Look at Effect on All Image Pixels | 19 |
| 4.5.2 | Look at Effect on Pixels That Only Contain Concrete | 19 |

| | |
|----------------------|-----------|
| <i>CONTENTS</i> | 2 |
| 5 Conclusions | 22 |
| 6 References | 23 |

List of Figures

| | | |
|----|---|----|
| 1 | Atmospheric transmission spectra showing windows available for earth observations. | 6 |
| 2 | Test image used for OSP evaluation (400×400). | 11 |
| 3 | Test image pixels convolved down to 10×10 | 11 |
| 4 | Spectral signature of 3 materials or endmembers and gaussian noise. | 13 |
| 5 | Classified concrete image, a) 10×10 and b) 400×400 pixels. | 16 |
| 6 | Classified a) tree-leaf and b) dirt images. | 16 |
| 7 | Classified concrete image with 1% noise present. | 17 |
| 8 | Classified a) tree-leaf and b) dirt images with 1% noise present. 17 | |
| 9 | Classified concrete image with 5% noise present. | 18 |
| 10 | Classified a) tree-leaf and b) dirt images with 5% noise present. 18 | |
| 11 | Normalized energy for classified concrete, as a function of noise, on a per-pixel basis. | 20 |
| 12 | Normalized energy for classified concrete showing actual data reflectance data points for the no-noise curve. | 20 |
| 13 | Plot illustrating | 22 |

List of Tables

| | | |
|---|--|----|
| 1 | The mixture fractions of 16 selected pixels from the test image. | 21 |
| 2 | Error associated with applying 1% and 5% noise to the image. | 23 |

1 Introduction

Remote sensing technology is concerned with the determination of characteristics of physical objects through the analysis of measurement taken at a distance from these objects. One important problem in remote sensing is the characterization and classification of (spectral) measurements taken from various situations on the earth surface. For example, based on certain spectral measurements, we may want to classify various crops planted in a particular region, or we would like to identify one or several specific soil types in a region from the spectral measurements [1]. Data can be collected in a few (multispectral) to as many as 200 (hyperspectral) spectral bands. Classification of a hyperspectral image data amounts to identifying which pixels contain various spectrally distinct materials that have been specified by the user. Classification approaches such as minimum distance to the mean (MDM) and Gaussian maximum likelihood (GML) [2] can be applied to this data as well as correlation/matched filter-type approaches such as spectral signature matching [3] and spectral angle mapper [4]. However, these techniques have difficulty accounting for mixed pixels (pixels that contain multiple spectral classes). A possible solution is to use the concept of orthogonal subspace projection (OSP) [5], [6]. This can be done by finding a matrix operator that eliminates undesired signatures in the data and then finding a vector operator which maximizes the residual desired signature signal-to-noise ratio (SNR). This, in turn, will produce a new set of images which highlight the presence of each signature of interest. At the same time, the orthogonal subspace projection technique will reduce the dimensionality of the hyperspectral data, which maybe more appealing to the analysts.

2 Background

2.1 Remote Sensing: An Overview

Remote sensing, for all practical purposes, is the field of study associated with extracting information about an object without coming into physical contact with it [7]. A definition such as this can include a multitude of disciplines such as medical imaging, astronomy, vision, sonar, and earth observation from above via an aircraft or space satellite. For the most part, remote sensing is often thought of in the latter context, viewing and analyzing earth from above.

The field of remote sensing is rather young, being about 30 years old or so. This goes back to the late 40's and early 50's when some of the first

satellite photographs were being recovered from V-2 launches. During this time the satellite imaging of the earth developed hand in hand with the international space program. Following the first manmade satellite launch of Sputnik 1 on October 4, 1957, photographs and video images were acquired by U.S. Explorer and Mercury programs and the Soviet Union's LUNA series. Just 3 years after Sputnik 1's debut (April 1960), the U.S. initiated its spaced-based reconnaissance program acquiring high-resolution photographic images from space [8]. Today remote sensing is used in a variety of applications such as environmental mapping, global change research, geological research, wetlands mapping, assessment of trafficability, plant and mineral identification and abundance estimation, and crop analysis.

In general, remote sensing enables us to look at the earth from a different point of view. This different vantage point can aid analysts and alike in making improved decisions or assessments. Furthermore, remote sensing technology enables us to view the earth through "windows" of the EM spectrum that would not otherwise be humanly possible. Figure 1 shows the transmission spectra of the earth's atmosphere. From this, it is clear that there are some regions or windows in the EM spectrum that have a higher transmission than others. These are what folks in the remote sensing community term "spectral bands". The earth can appear quite different depending on which band it is viewed in. Only recently have we been able to capture a multitude of high resolution spectral bands at once. Such devices that seize this high resolution imagery are called imaging spectrometers.

2.2 Sensors and Imaging Spectrometers

One of the most important parts of the remote imaging system is the sensor. The imaging system must have some type of sensing mechanism to capture EM radiation. These mechanisms can be analog or digital. Some imagers use film while others use CCD arrays. These instrument or sensor platforms can be divided into those with one to ten or so spectral channels (multispectral) and those with tens to hundreds of spectral channels (hyperspectral). The focus here is on the latter. Advances in sensor design have paved the way for a new generation of sensors called imaging spectrometers. Imaging spectrometry has been under development since the 1970's as a means of identifying and mapping earth resources. As a result, hyperspectral data permit the expansion of detection and classification activities to targets previously unresolved in multispectral images. In spectroscopy, reflectance variation as a function of wavelength provides a unique signature, or fingerprint, that can be used to identify materials. Imaging spectrometry

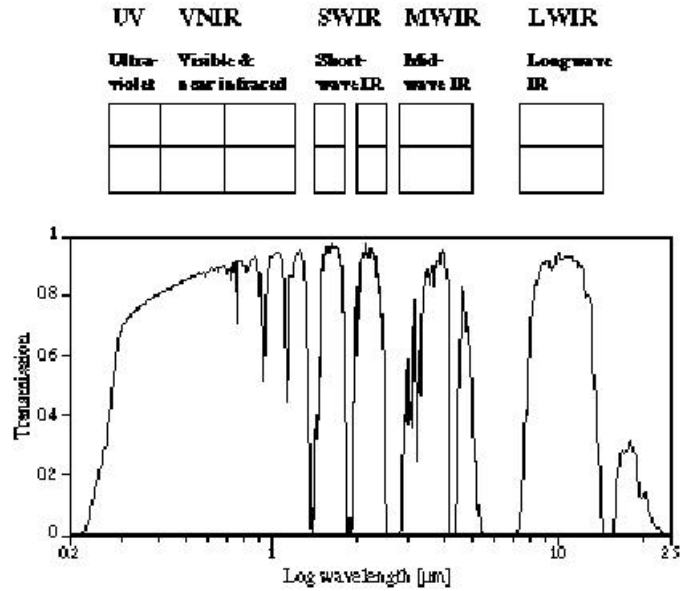


Figure 1: Atmospheric transmission spectra showing windows available for earth observations.

ters go one step further, imaging a scene with high spatial resolution and over many discrete wavelength bands so that absorption features can be assigned to distinct geographic elements such as vegetation, rock, or urban development. One such sensor is the Airborne Visible InfraRed Imaging Spectrometer (AVIRIS) which images in 224 bands from 400 to 2500nm.

2.3 Classification Techniques and Transforms

With the increased use of hyperspectral image data comes the need for more efficient tools that can dimensionally reduce, classify, and reveal important information content of the data. As previously mentioned, classification of a hyperspectral image data amounts to identifying which pixels contain various spectrally distinct materials that have been specified by the user. There has been numerous techniques applied to this data such as minimum distance to the mean (MDM), Gaussian maximum likelihood (GML) [2], and correlation/matched filter-type approaches such as spectral signature matching [3] and spectral angle mapper [4], [9]. The MDM and GML classifiers have difficulty accounting for mixed pixels (pixels that contain multiple spectral classes), though there have been attempts to improve this for hy-

perspectral data [10]. Correlation and match filtering techniques have the same mixed pixel problem as well as the limitation that the output of the matched filter is nonzero and quite often large for multiple classes [5].

Various transforms can be used to reduce the dimensionality of the data. One of the more common linear transforms is the principle components (PC) transformation. It is designed to decorrelate the data and maximize the information content in a reduced number of features. A recent improvement to the PC transformation is the noise-adjusted PC transformation [12]. This transformation orders the new images in terms of SNR, and thus de-emphasizes noise in the resulting images [13]. While these techniques are adequate for reducing data dimensionality, they lack the ability to accentuate spectral signatures of interest. A possible solution to this problem is the use of orthogonal subspace projections (OSP).

3 Orthogonal Subspace Projection Classification

3.1 Problem Formation

The idea of the orthogonal subspace projection classifier is to eliminate all unwanted or undesired spectral signatures (background) within a pixel, then use a matched filter to extract the desired spectral signature (endmember) present in that pixel.

To start with we formulate the problem at hand. In hyperspectral image analysis, the spatial coverage of each pixel, more often than not, may encompass several different materials. Such a pixel is called a “mixed” pixel. It contains multiple spectral signatures. To start with, we formulate and describe a column vector \mathbf{r}_i to represent the mixed pixel by the linear model:

$$\mathbf{r}_i = \mathbf{M}\alpha_i + \mathbf{n}_i \quad (1)$$

In this treatment it should be noted that *vectors* are in lower case bold typeface while *matrices* are in upper case bold. As Tu *et al* [6] point out, let the vector \mathbf{r}_i be a $\ell \times 1$ column vector and denote the i^{th} mixed pixel in a hyperspectral image, where ℓ is the number of spectral bands.

Each distinct material in the mixed pixel is called an *endmember* (p). We assume there are p spectrally distinct endmembers in the i^{th} mixed pixel. The column vector \mathbf{r}_i can be in digital counts (DC), radiance, or reflectance depending on how endmembers and noise are defined.

Now assume that the matrix \mathbf{M} , of dimension $\ell \times p$, is made up of linearly independent columns. These columns are denoted $(\mathbf{m}_1, \mathbf{m}_2, \dots, \mathbf{m}_j, \dots, \mathbf{m}_p)$

where $\ell > p$ (overdetermined system) and \mathbf{m}_j is the spectral signature of the j^{th} distinct material or endmember. Let α_i be a p column vector given by $(\alpha_1, \alpha_2, \dots, \alpha_j, \dots, \alpha_p)^T$ where the j^{th} element represents the *fraction* of the j^{th} signature present in the i^{th} mixed pixel. This is a vector of endmember fractions.

Finally we consider additive noise. Let \mathbf{n}_i be a $\ell \times 1$ column vector representing additive white gaussian noise with zero mean and covariance matrix $\sigma^2 \mathbf{I}$, where \mathbf{I} is an $\ell \times \ell$ identity matrix.

In this representation we assume \mathbf{r}_i is a linear combination of p endmembers with the weight coefficients designated by the abundance (fraction) vector α_i . We can rewrite the term $\mathbf{M}\alpha_i$ so as to separate the desired spectral signatures from the undesired signatures. Simply put, we are separating the target from the background. For brevity we omit the subscript i representing the calculation on a *per pixel* basis. In searching for a *single spectral signature* we write:

$$\mathbf{M}\alpha = \mathbf{d}\alpha_p + \mathbf{U}\gamma \quad (2)$$

where \mathbf{d} is $\ell \times 1$, the desired signature of interest containing column vector \mathbf{m}_p while α_p is 1×1 , the fraction of the desired signature. The matrix \mathbf{U} is composed of the remaining column vectors from \mathbf{M} . These are the undesired spectral signatures or background information. This is given by $\mathbf{U} = (\mathbf{m}_1, \mathbf{m}_2, \dots, \mathbf{m}_j, \dots, \mathbf{m}_{p-1})$ with dimension $\ell \times (p-1)$ where γ is a column vector which contains the remaining $(p-1)$ components (fractions) of α . That is $\gamma = (\alpha_1, \alpha_2, \dots, \alpha_j, \dots, \alpha_p)^T$.

3.2 Hyperspectral Pixel Classification

3.2.1 Interference Rejection by Orthogonal Subspace Projection

We can now develop an operator \mathbf{P} which eliminates the effects of \mathbf{U} , the undesired signatures. To do this we develop an operator that projects \mathbf{r} onto a subspace that is orthogonal to the columns of \mathbf{U} . This results in a vector that only contains energy associated with the target \mathbf{d} and noise \mathbf{n} . This is done by using a *least squares optimal interference rejection operator* [5], [6]. The operator used is the $\ell \times \ell$ matrix

$$\mathbf{P} = (\mathbf{I} - \mathbf{U}\mathbf{U}^\dagger) \quad (3)$$

where \mathbf{U}^\dagger is the pseudo inverse of \mathbf{U} , denoted $\mathbf{U}^\dagger = (\mathbf{U}^T\mathbf{U})^{-1}\mathbf{U}^T$. The operator \mathbf{P} maps \mathbf{d} into a space orthogonal to the space spanned by the

uninteresting signatures in \mathbf{U} . We now operate on the mixed pixel \mathbf{r} from Equation 1.

$$\mathbf{Pr} = \mathbf{Pd}\alpha_p + \mathbf{PU}\gamma + \mathbf{Pn} \quad (4)$$

It should be noticed that \mathbf{P} operating on $\mathbf{U}\gamma$ reduces the contribution of \mathbf{U} to zero (close to zero in real data applications). Therefore, upon rearrangement we have

$$\mathbf{Pr} = \mathbf{Pd}\alpha_p + \mathbf{Pn} \quad (5)$$

This is an optimal interference rejection process in the least squares sense.

3.2.2 Signal-to-Noise Ratio (SNR) Maximization

We now want to find an operator \mathbf{x}^T which will maximize the signal-to-noise ratio (SNR). The operator \mathbf{x}^T acting on \mathbf{Pr} will produce a scalar.

$$\lambda = \frac{\mathbf{x}^T \mathbf{Pd}\alpha_p^2 \mathbf{d}^T \mathbf{P}^T \mathbf{x}}{\mathbf{x}^T \mathbf{PE}\{\mathbf{nn}^T\} \mathbf{P}^T \mathbf{x}} \quad (6)$$

$$\lambda = \left(\frac{\alpha_p^2}{\sigma^2} \right) \frac{\mathbf{x}^T \mathbf{P} \mathbf{d} \mathbf{d}^T \mathbf{P}^T \mathbf{x}}{\mathbf{x}^T \mathbf{P} \mathbf{P}^T \mathbf{x}} \quad (7)$$

where $\mathbf{E}\{\}$ denotes the expected value. Maximization of this quotient is the generalized eigenvector problem

$$\mathbf{P} \mathbf{d} \mathbf{d}^T \mathbf{P}^T \mathbf{x} = \tilde{\lambda} \mathbf{P} \mathbf{P}^T \mathbf{x} \quad (8)$$

where $\tilde{\lambda} = \lambda(\sigma^2/\alpha_p)$. The value of \mathbf{x}^T which maximizes $\tilde{\lambda}$ can be determined in general using techniques outlined in [14] and the idempotent ($\mathbf{P}^2 = \mathbf{P}$) and symmetric ($\mathbf{P}^T = \mathbf{P}$) properties of the interference rejection operator. As it turns out the value of \mathbf{x}^T which maximizes the SNR is

$$\mathbf{x}^T = k \mathbf{d}^T \quad (9)$$

where k is an arbitrary scalar. This leads to an overall classification operator for a desired hyperspectral signature in the presence of multiple undesired signatures and white noise. This is given by the $1 \times \ell$, vector

$$\mathbf{q}^T = \mathbf{d}^T \mathbf{P} \quad (10)$$

This result first nulls the interfering signatures, and then uses a matched filter for the desired signature to maximize the SNR. When the operator is applied to all of the pixels in a hyperspectral scene, each $\ell \times 1$ pixel is reduced to a scalar which is a measure of the presence of the signature of interest. The ultimate result is to reduce the ℓ images that make-up the hyperspectral image cube into a single image where pixels with high intensity indicate the presence of the desired signature.

This operator can be easily extended to seek out k signatures of interest. The vector operator simply becomes a $k \times \ell$ matrix operator which is given by

$$\mathbf{Q} = (\mathbf{q}_1, \mathbf{q}_2, \dots, \mathbf{q}_i, \dots, \mathbf{q}_k)^T \quad (11)$$

where each of the $\mathbf{q}_i^T = \mathbf{d}_i^T \mathbf{P}_i$ is formed with the appropriate desired and undesired signature vectors. In this case, the hyperspectral image cube is reduced to k images which classify each of the signatures of interest.

4 100 Pixel Simulated Scene

4.1 Scene Overview

A sample image (10×10) with *linearly* mixed pixels was created in order to verify the functionality of the OSP operator. This image or *image cube* consisted of 16 spectral bands ($0.5\mu m$ to $2.0\mu m$) and 3 endmembers or classes (concrete, tree leaf, and dirt). The endmember vectors contained reflectance values that were representative of the various materials. Gaussian normally distributed noise was also added to the vectors. One data set was run without noise. A second data set contained noise, $n(\mu = 0, \sigma = 0.01)$ while a third contained noise, $n(\mu = 0, \sigma = 0.05)$.

The hypothetical hi-res image (400×400) resembles a road with a tree line on both sides of it. Outside of the tree line are open areas of dirt. One band of the image can be seen in Figure 2 where the darkest pixels are concrete, the lightest pixels are dirt, and the middle shade of grey are trees.

In general, the pixel size in the final output image is a function of the detector element size. If we wish to work with a 10×10 image, we will have to convolve or degrade the test scene. With this in mind, the test image would actually look like the one in Figure 3. This process gives us our mixed pixel test image.

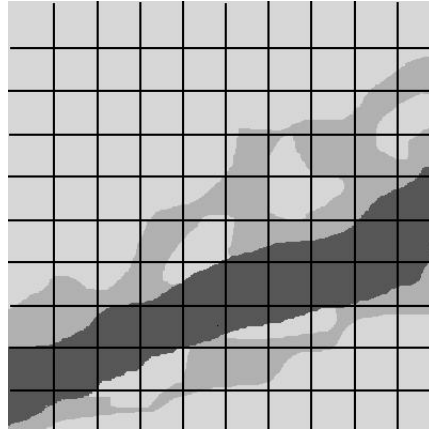


Figure 2: Test image used for OSP evaluation (400×400).

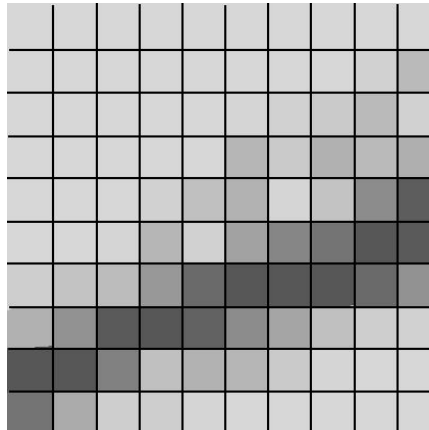


Figure 3: Test image pixels convolved down to 10×10 .

4.2 OSP Formulation and Results for One Pixel w/o Noise

We start with 3 vectors or classes, each 16 elements or bands long. The vectors are in reflectance units and can be seen below. A graphical representation of these vector is illustrated in Figure 4 along with a curve of 5% gaussian noise.

$$\begin{array}{l}
 \begin{array}{c}
 \left[\begin{array}{c}
 0.26 \\
 0.30 \\
 0.31 \\
 0.31 \\
 0.31 \\
 0.31 \\
 0.34 \\
 0.34 \\
 0.33 \\
 0.32 \\
 0.33 \\
 0.34 \\
 0.35 \\
 0.34 \\
 0.28 \\
 0.27
 \end{array} \right] \\
 \text{Concrete} =
 \end{array}
 \end{array}
 \begin{array}{c}
 \begin{array}{c}
 \left[\begin{array}{c}
 0.07 \\
 0.07 \\
 0.11 \\
 0.54 \\
 0.55 \\
 0.54 \\
 0.56 \\
 0.50 \\
 0.49 \\
 0.18 \\
 0.19 \\
 0.30 \\
 0.32 \\
 0.28 \\
 0.05 \\
 0.10
 \end{array} \right] \\
 \text{Treeleaf} =
 \end{array}
 \end{array}
 \begin{array}{c}
 \begin{array}{c}
 \left[\begin{array}{c}
 0.07 \\
 0.13 \\
 0.19 \\
 0.25 \\
 0.30 \\
 0.34 \\
 0.38 \\
 0.40 \\
 0.42 \\
 0.42 \\
 0.44 \\
 0.45 \\
 0.46 \\
 0.46 \\
 0.40 \\
 0.42
 \end{array} \right] \\
 \text{Dirt} =
 \end{array}
 \end{array}
 \end{array}$$

We now need to define the fraction mixtures of each of the 100 pixels in Figure 2 (on page 11) starting from left-to-right, top-to-bottom. For example, the model for pixel 40 (last pixel in the 4th row) might look like,

$$\text{pixel40} \equiv (0.08)\text{concrete} + (0.75)\text{treeleaf} + (0.17)\text{dirt} + \text{noise}$$

Where noise, in this first case, is zero. Once all the pixel mixture fractions have been defined, we can choose a particular class spectra to extract from the test image. For the first image we will develop an algorithm using the OSP operator to extract the material *concrete* from all the pixels throughout the test image. This same procedure will then be used to extract the grass and dirt materials.

To start, we will develop the algorithm for one particular pixel and then apply the same technique to the remaining pixels. For example, we assume

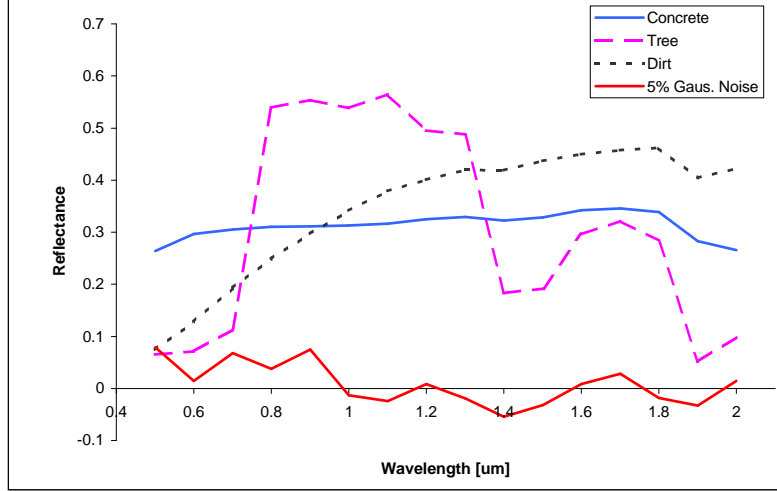


Figure 4: Spectral signature of 3 materials or endmembers and gaussian noise.

that pixel 40 is made up of some weighted linear combination of endmembers and noise.

$$\mathbf{pixel40} = \mathbf{M}\alpha + \mathbf{noise} \quad (12)$$

Furthermore, we can break up $\mathbf{M}\alpha$ into desired, $\mathbf{d}\alpha_p$ and undesired, $\mathbf{U}\gamma$ signatures.

$$\mathbf{pixel40} = \mathbf{d}\alpha_p + \mathbf{U}\gamma + \mathbf{noise} \quad (13)$$

Now we assign the desired, \mathbf{d} and undesired, \mathbf{U} signatures to spectra. We let concrete be the vector \mathbf{d} and tree-leaf and dirt be the column vectors of the matrix \mathbf{U} . However, we don't know the fractions. We just know pixel 40 is made up of some combination of \mathbf{d} and \mathbf{U} .

$$\mathbf{d} \equiv [\mathit{concrete}] \quad \mathbf{U} \equiv [\mathit{treeleaf}, \mathit{dirt}]$$

We ultimately want to reduce the effects of \mathbf{U} . To do this we need to find a projection operator \mathbf{P} , that when operated on \mathbf{U} , will reduce its contribution to zero. Ultimately we want $\mathbf{U} - \mathbf{U} = \mathbf{O}$, the null matrix. If \mathbf{U} were symmetric we could use the operator $\mathbf{P} = \mathbf{I} - \mathbf{U}\mathbf{U}^{-1}$. This would yield

$$(\mathbf{I} - \mathbf{U}\mathbf{U}^{-1})\mathbf{U} = (\mathbf{I} - \mathbf{I})\mathbf{U} = \mathbf{U} - \mathbf{U} = \mathbf{O} \quad (14)$$

However, \mathbf{U} will more than likely be asymmetric. So we need to use the pseudoinvers, \mathbf{U}^\dagger in place of \mathbf{U}^{-1} .

$$\mathbf{U}^\dagger = (\mathbf{U}^T\mathbf{U})^{-1}\mathbf{U}^T \quad (15)$$

The projection operator now becomes

$$\mathbf{P} = \mathbf{I} - \mathbf{U}\mathbf{U}^\dagger \quad (16)$$

where \mathbf{I} is the identity matrix

To find concrete, \mathbf{d} , we project pixel 40 onto a subspace that is orthogonal to the columns of \mathbf{U} using the operator \mathbf{P} . In other words, \mathbf{P} maps \mathbf{d} into a space orthogonal to the space spanned by the undesired signatures while simultaneously minimizing the effects of \mathbf{U} .

If we operate on \mathbf{U} , which contains tree-leaf and dirt, with \mathbf{P} , we can see that it does a good job at minimizing the effects of \mathbf{U} .

$$\mathbf{P}\mathbf{U} = \begin{bmatrix} 0 & 0 \\ 0 & 0 \\ 0 & 0 \\ 0 & 0 \\ 0 & 0 \\ 0 & 0 \\ 0 & 0 \\ 0 & 0 \\ 0 & 0 \\ 0 & 0 \\ 0 & 0 \\ 0 & 0 \\ 0 & 0 \\ 0 & 0 \\ 0 & 0 \\ 0 & 0 \\ 0 & 0 \\ 0 & 0 \\ 0 & 0 \\ 0 & 0 \end{bmatrix}$$

If we let $\mathbf{r}_1 =$ pixel 40 and $\mathbf{n} =$ noise, we have from Equation 5

$$\mathbf{P}\mathbf{r}_1 = \mathbf{P}\mathbf{d}\alpha_p + \mathbf{P}\mathbf{n} \quad (17)$$

We now want to find an operator \mathbf{x}^T which will maximize the signal-to-noise ratio (SNR). The operator \mathbf{x}^T acting on $\mathbf{P}\mathbf{r}_1$ will produce a scalar. As stated before, the value of \mathbf{x}^T which maximizes the SNR is

$$\mathbf{x}^T = k\mathbf{d}^T \quad (18)$$

where k is an arbitrary scalar. This leads to the overall OSP operator

$$\mathbf{d}^T\mathbf{P}\{\} \quad (19)$$

For pixel 40, which has 8% concrete, 75% tree-leaf, and 17% dirt, the energy result is

$$(\mathbf{d}^T\mathbf{P})\mathbf{r}_1 = 5.19$$

The output of the OSP operator is just a scalar that is proportional to the energy we are seeking. In this case it was concrete from pixel 40.

4.3 OSP Results for Test Image with out Noise

We now wish to apply the operator image wide, so as to classify concrete, tree-leaf, and dirt, respectively. Again, the operator is applied to each pixel and a scalar is generated. The scalar is a function of the energy associated with the signature of interest. Some pixels in the test scene in Figure 3 are pure concrete while others are a combination of the 3 materials and potential noise.

The initial classification was done using concrete as the desired, \mathbf{d} signature and tree-leaf and dirt as the undesired signatures, \mathbf{U} . The result of this can be seen in Figure 5 where we have up-convolved the image back to 400×400 pixels.

The abundance of concrete (the desired signature) is directly proportional to the brightness of the pixel. Black pixels contain no concrete while pure white pixels are made up entirely of concrete.

Similarly, the operator was then used to classify tree-leaf and dirt. The relationship between abundance and brightness holds true for these examples as well. These results can be seen in Figure 6.

We see that the OSP operator has done a very good job of extracting the 3 different material types from the test image. This is expected, however. If we look at pixel 40 again, we know it had 8% concrete in it. For the noiseless case, the normalized concrete energy will correlate exactly with the

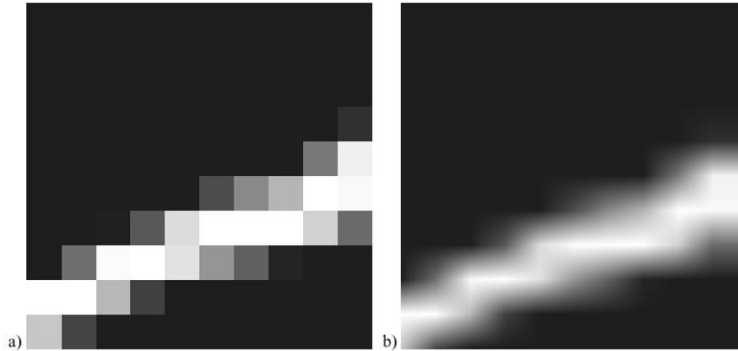


Figure 5: Classified concrete image, a) 10×10 and b) 400×400 pixels.

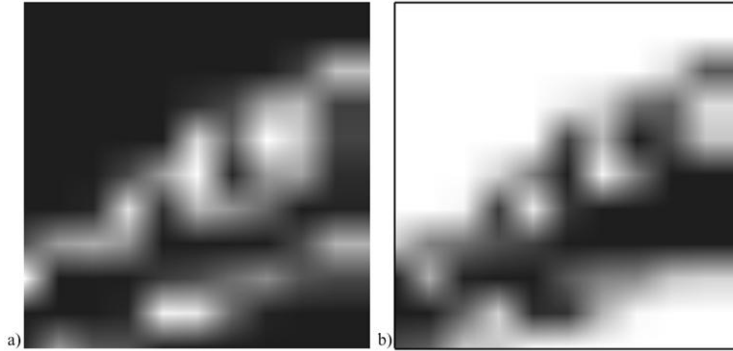


Figure 6: Classified a) tree-leaf and b) dirt images.

normalized concrete reflectance. Therefore, the error between the reflectance and normalized concrete energy will be zero. This would be expected since the values that make up the \mathbf{U} matrix are *exactly* the truth signatures in the image. The normalization here assumes that the maximum concrete energy value came from a pixel that was 100% concrete.

4.4 OSP Results for Test Image with Noise

4.4.1 1% Gaussian Noise

We now look at the performance of the OSP operator in the presence of noise. The noise distribution added to the vector set was random gaussian distributed noise with $\mu = 0$ and $\sigma = 0.01$. The results of this on the test

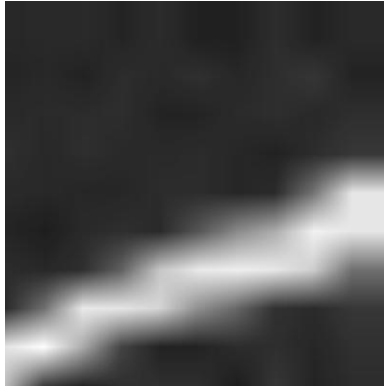


Figure 7: Classified concrete image with 1% noise present.

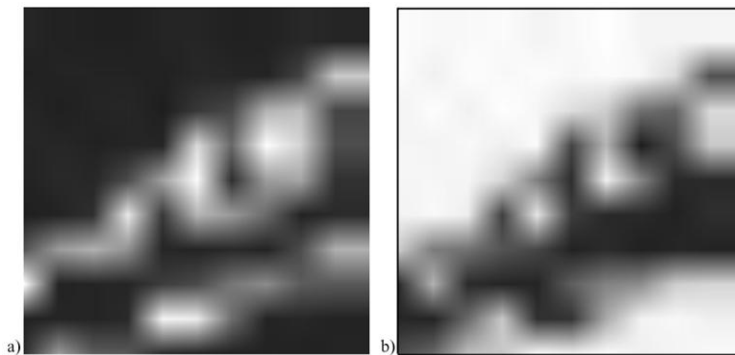


Figure 8: Classified a) tree-leaf and b) dirt images with 1% noise present.

image can be seen in Figures 7 and 8.

Noise at the 1% level has not affected the results that much. The classifications look very similar to the noise-less cases. One exception can be seen in the dirt classification of Figure 8, however. We can see that there is a little bit of uncertainty in the open dirt areas. The pixels in this region are slightly darker than the ones in the similar, noise-less case, of Figure 6.

4.4.2 5% Gaussian Noise

In this last set of images we add noise with $\mu = 0$ and $\sigma = 0.05$. This value of 5% is approaching the baseline reflectance for some of the endmembers in Figure 4. In the $1.6\mu\text{m}$ to $1.8\mu\text{m}$ range, the 5% noise may actually have the

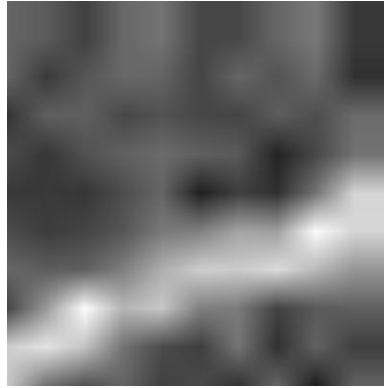


Figure 9: Classified concrete image with 5% noise present.

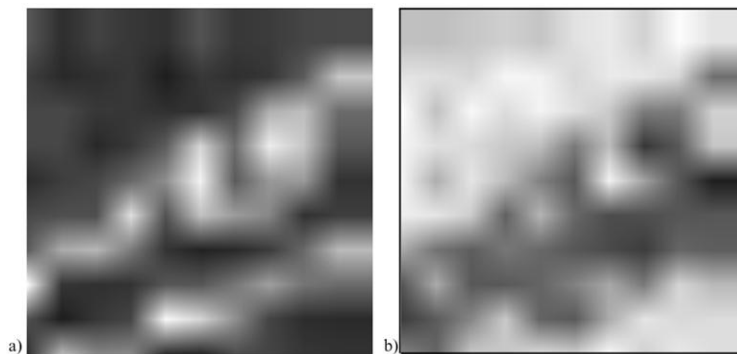


Figure 10: Classified a) tree-leaf and b) dirt images with 5% noise present.

ability to completely mix-up or distort the tree-leaf and concrete spectra. The results of this experiment can be seen in Figures 9 and 10.

It is evident from the images that noise at the 5% level has played a major role in the classification results. As an example, some of the dirt areas have been falsely identified as concrete in Figure 9. However, even with noise at this level, the three classes can still be differentiated from the background.

4.5 Classified Concrete Image: A Closer Look at Noise

4.5.1 Look at Effect on All Image Pixels

In this section we examine the effects of noise on the classified concrete images presented earlier. Figure 11 shows a plot of energy v.s. pixel location. This is generated by simply scanning across the rows of the classified image and recording the energy values. The values are then placed end-to-end and the plot in Figure 11 is thus created.

This plot gives us another quantitative look at the classified data and how it behaves in the presence of noise. The normalization in this plot is based on the energy value from a pure concrete pixel with out noise. All other energy values are therefore relative to this.

The effect of adding 1% noise is now more apparent than was seen in Figure 7. Again, this is the same data as Figure 7, just viewed as a plot instead of an 8-bit image. We see that the areas that contained pure dirt spectra (pixels 0 to 39), now show variability in energy where there should be none. This variability observation was not as obvious in Figure 7.

What is evident in both Figure 9 and Figure 11, is the effect of adding in 5% noise. It is seen that the variability due to noise may mask some features that have a reflectivity of less than 20%. This can be seen in Figure 12. For example, we can clearly see that the magnitude of the noise dominates pixel 40, which had 8% concrete in it.

4.5.2 Look at Effect on Pixels That Only Contain Concrete

We now take a closer look at a subset of pixels that *only* contain concrete. We choose a total of 16 pixels that range from 100% to 1% concrete. These pixels, along with their percentages of tree-leaf and grass, can be seen in Table 1.

We then look at the energy result of the OSP operator for each concrete percentage as a function of applied noise. The result of this can be seen in Figure 13. Again the energy is normalized relative to the no-noise maximum value, which contained 100% concrete.

As expected, we see a perfect one-to-one mapping of concrete percentage to normalized energy (the solid black line in Figure 13). That is, the calculated energy from the operator is (perfectly) linearly related to the amount of concrete in it. Therefore, we have an ideal straight line with a slope of 0.01 and intercept of 0.0. If concrete, in this Figure, was written as a fraction instead of a percent, the slope would simply be one.

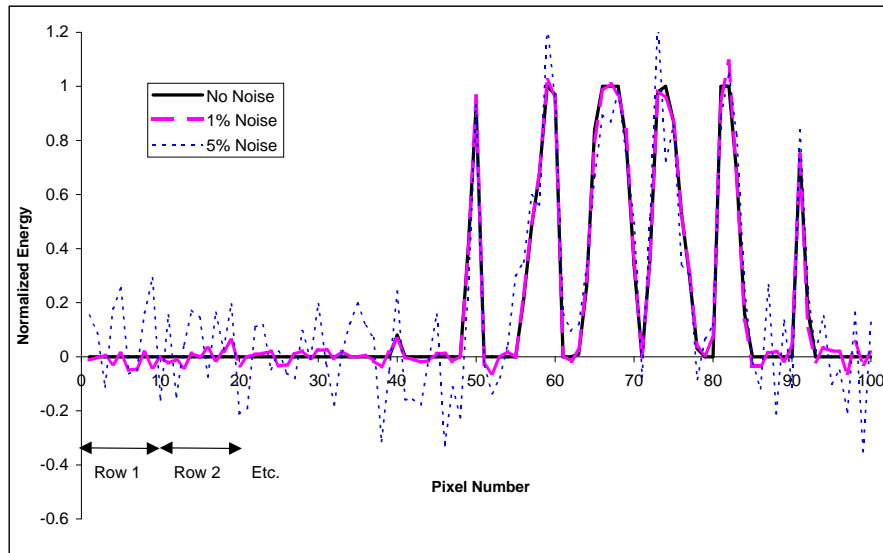


Figure 11: Normalized energy for classified concrete, as a function of noise, on a per-pixel basis.

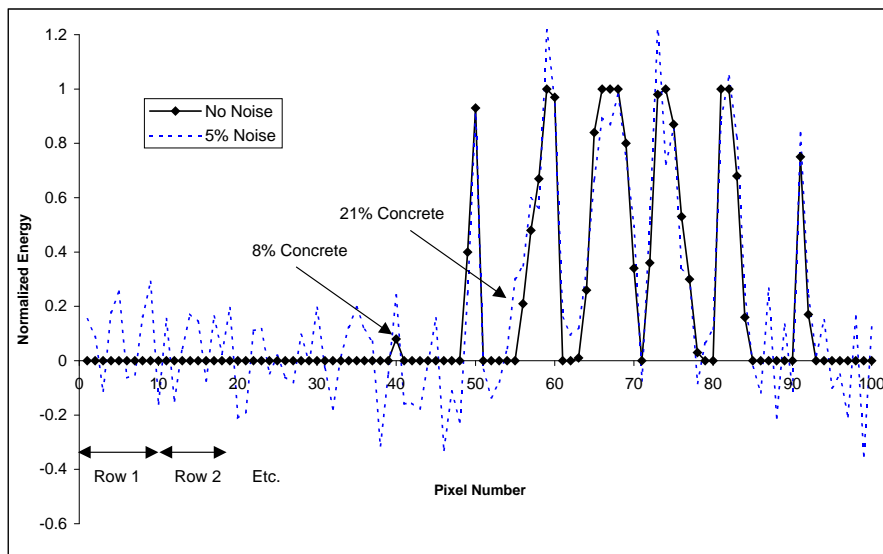


Figure 12: Normalized energy for classified concrete showing actual data reflectance data points for the no-noise curve.

Table 1: The mixture fractions of 16 selected pixels from the test image.

| Pixel Number | Concrete [%] | Tree-leaf [%] | Dirt [%] |
|--------------|--------------|---------------|----------|
| 59 | 100 | 0 | 0 |
| 50 | 93 | 0 | 7 |
| 65 | 84 | 16 | 0 |
| 69 | 80 | 0 | 20 |
| 91 | 75 | 20 | 5 |
| 58 | 67 | 0 | 33 |
| 76 | 53 | 27 | 20 |
| 57 | 48 | 0 | 52 |
| 49 | 40 | 0 | 60 |
| 70 | 34 | 0 | 66 |
| 64 | 26 | 22 | 52 |
| 56 | 21 | 11 | 68 |
| 92 | 17 | 29 | 54 |
| 40 | 8 | 75 | 17 |
| 78 | 3 | 48 | 49 |
| 63 | 1 | 36 | 63 |

Once we add noise, 1% and 5%, to the pixels, we see that the energy values deviate significantly. As expected, the energy return with 1% noise in it, stays fairly close to the 1:1 line, but tends to deviate more at the lower percentages. Similarly, the energy associated with the 5% noise contribution has the same behavior but on a larger scale.

We can see the magnitude of these errors numerically by looking at Table 2. Here we have normalized the selected concrete pixel energy's while simultaneously computing a proportional error, ε using the relation

$$\varepsilon = \frac{|E_0 - E_x|}{E_0} 100 \quad (20)$$

where E_0 is the energy associated with the no-noise case and E_x is either the energy from the 1% or 5% noise cases. If we omit the last few error terms and compute an average error (using the 100% to 26% concrete values), we find an average error of 6% for the 1% noise case and 17% for the more variable 5% case.

Overall we can see that that OSP operator did a fairly good job of extracting concrete from the other signatures in the presence of noise, with moderate success at the 5% level. However, we see that the errors are fairly significant at percentages below 26% and extremely high at values below 8% concrete, especially in the 5% noise case. Again, if there wasn't any noise in the data, the normalized concrete energy would correlate exactly with the

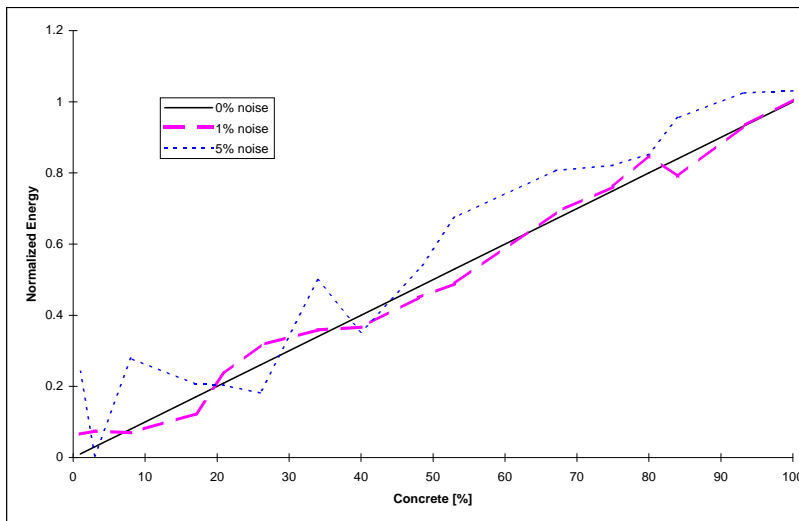


Figure 13: OSP operator result for concrete only as a function of noise.

normalized concrete percentages, thus driving the error to zero.

5 Conclusions

The OSP operator can be viewed as a combination of two linear operators into a single classification operator. The first operator is an optimal interference rejection process in the least squares sense, and the second is an optimal detector in the maximum SNR sense. This technique does not suffer from the limitations of standard statistical classifiers and matched filtering/spectral signature matching techniques which are suboptimal in the presence of multiple correlated interferers.

Though the technique is fairly robust, there are some limitations to this approach. You need to know the end member vectors that make up the \mathbf{d} vector and \mathbf{U} matrix. However, the endmembers don't necessarily need to be identified, they can be image derived (*e.g.*, using the pixel purity index algorithm (PPI)). Also, if your target looks like an endmember, you may have suppressed it in the suppression step. Since noise is assumed to be independent, identically distributed (i.i.d), you have to work in a space where this is approximately true, *i.e.*, image DC or radiance space. Transforming to reflectance space may distort noise and invalidate this approach, though we did not perform any transforms for we started in reflectance space.

Table 2: Error associated with applying 1% and 5% noise to the image.

| Pixel Number | Concrete [%] | Norm Energy 0% Noise | Norm Energy 1% Noise | Norm Energy 5% Noise | 1% Noise Error [%] | 5% Noise Error [%] |
|--------------|--------------|----------------------|----------------------|----------------------|--------------------|--------------------|
| 59 | 100 | 1.00 | 1.01 | 1.03 | 0.5 | 3.1 |
| 50 | 93 | 0.93 | 0.93 | 1.03 | 0.0 | 10.2 |
| 65 | 84 | 0.84 | 0.79 | 0.96 | 5.9 | 13.7 |
| 69 | 80 | 0.80 | 0.85 | 0.85 | 6.3 | 6.7 |
| 91 | 75 | 0.75 | 0.76 | 0.82 | 1.5 | 9.5 |
| 58 | 67 | 0.67 | 0.69 | 0.81 | 2.7 | 20.4 |
| 76 | 53 | 0.53 | 0.49 | 0.67 | 7.8 | 27.3 |
| 57 | 48 | 0.48 | 0.45 | 0.53 | 6.4 | 9.5 |
| 49 | 40 | 0.40 | 0.37 | 0.35 | 8.4 | 11.7 |
| 70 | 34 | 0.34 | 0.36 | 0.50 | 5.6 | 46.9 |
| 64 | 26 | 0.26 | 0.32 | 0.18 | 21.4 | 30.1 |
| 56 | 21 | 0.21 | 0.24 | 0.20 | 12.9 | 3.1 |
| 92 | 17 | 0.17 | 0.12 | 0.21 | 27.7 | 21.7 |
| 40 | 8 | 0.08 | 0.07 | 0.28 | 12.5 | 249.0 |
| 79 | 3 | 0.03 | 0.07 | 0.01 | 148.2 | 82.9 |
| 63 | 1 | 0.01 | 0.07 | 0.24 | 560.4 | 2315.0 |

References

6 References

- [1] Fu, K.S., Applications of Pattern Recognition, Florida: CRC Press, Inc., 1982.
- [2] Swain, P., Davis, E.S., Remote Sensing: The Quantitative Approach. New York: McGraw-Hill, 1983.
- [3] Mazer, A.S., Martin, M., et al., "Image processing software for imaging spectrometry data analysis," Remote Sensing of Environment, vol. 24. no. 1, pp. 201-210, 1988.
- [4] Yuhas, R.H., Goetz, A.F.H., Boardman, J.W., "Discrimination among semi-arid landscape endmembers using the spectral angle mapper (SAM) algorithm," Summaries 3rd Annual JPL Airborne Geoscience Workshop, Jun 1992, R.O. Green, Ed., Publ. 92-14, vol. 1, Jet Propulsion Laboratory, Pasadena, CA, 1992, pp. 147-149.
- [5] Harsanyi, J.C, Chang, C.-I, "Hyperspectral image classification and dimensionality reduction: An orthogonal subspace projection approach",

- IEEE Transactions on geoscience and remote sensing, vol. 32, pp. 779-785, July 1994.
- [6] Tu, T.-M, Chen, C.-H, Chang, C.-I, "A posteriori least squares orthogonal subspace projection approach to desired signature extraction and detection", IEEE Transactions on geoscience and remote sensing, vol. 35, pp. 127-139, January 1997.
- [7] Schott, J.R., Remote Sensing: The Image Chain Approach, New York, Oxford University Press, 1997.
- [8] McDonald, R.A., "Opening the cold war sky to the public: declassifying satellite reconnaissance imagery." Photogrammetric Engineering and Remote Sensing, vol. 61, no. 4, pp. 385-390, 1995.
- [9] Kruse, F.A., Lefkoff, A.B., Boardman, J.W., Heidebrecht, K.B., Shapiro, A.T., Barloon, P.J., Goetz, A.F.H., "The spectral image processing system (SIPS) interactive visualization and analysis of imaging spectrometer data." Remote Sensing of Environment, vol. 44, pp. 145-163, 1993.
- [10] Roger, R.E., "Sparse inverse covariance matrices and efficient maximum likelihood classification of hyperspectral data", International journal of remote sensing, vol. 17, pp. 589-613, June 1995.
- [11] Clark, R.N., Gallagher, A.J., Swayze, G.A., "Material absorption band depth mapping of imaging spectrometer data using a complete band shape least-squares fit with library reference spectra," AVIRIS workshop, Robert O. Green, ed., pp. 176-186. 1990.
- [12] Lee, J.B., Woodyatt, A.S., Berman, M., "Enhancement of high spectral resolution remote sensing data by a noise-adjusted principal components transform", IEEE Transactions on geoscience and remote sensing, vol. 28, pp. 295-304, May 1990.
- [13] Green, A.A, Berman, M., Switzer, P., Craig, M.D., "A transformation for ordering multispectral data in terms of image quality with implications for noise removal", IEEE Transactions on geoscience and remote sensing, vol. 26, pp. 65-74, January 1988.
- [14] Miller, J.W.V., Farison, J.B., Shin, Y., "Spatially invariant images sequences." IEEE Transactions on Image Processing, vol. 1, pp. 148-161, Apr. 1992.